Development of integrated effect plate for performance improvement of multi-effect diffusion solar still

Ga-Ram Lee[a,b], Tri Ayodha Ajiwiguna[b,c], Byung-Ju Lim[a], Chang-Dae Park[a,b,]*

[a]Korea Institute of Machinery & Materials, 156 Gajeongbuk-Ro, Yuseong-Gu, Daejeon 34103, Republic of Korea,
Tel. +010-4505-3935; email: parkcdae@kimm.re.kr (C.D. Park), Tel. +010-9470-0383;
email: ccl3455@kimm.re.kr (G.R. Lee), Tel. +010-2623-2432; email: bzoo77@kimm.re.kr (B.J. Lim)
[b]University of Science & Technology, 217 Gajeong-Ro, Yuseong-Gu, Daejeon 34113, Republic of Korea,
Tel. +010-3588-0802; email: TriAyodha@kimm.re.kr (T.A. Ajiwiguna)
[c]Telkom University, Engineering Physics Department, Jalan Telekomunikasi, Bandung 40257, Indonesia

ABSTRACT

This paper describes the development process and experimental results of the wick-free plate to improve the performance of the effect plate (wick-plate structure), which is a key component playing a role as both evaporation surface and condensation surface in multi-effect diffusion solar still (MED). The effect plates of the MED normally use a flat metal plate attached to a fabric wick on its one surface to secure the evaporation area and time. However, the process attaching the wick to the plate causes an increase in manufacturing time and cost, and detachment of the aged wick from the plate causes a decrease in the still's performance and reliability. To solve these problems, we have developed a wick-free plate without wick, which can replace the wick-plate. We selected seven characteristics required for the wick-free plate and fabricated wick-free plate specimens such as etching plate, 3D printing plate, and porous metal plate. Then, their performances were compared with the wick-plate by analyzing the characteristics. Experimental results showed that the etching plate of grooved shape is appropriate for wick-free plate and the optimum patterned shape of the grooved plate is 3.5 mm for the pitch, 3.0 mm for the furrow, and 2.0 mm for the depth. Outdoor performance experiment showed that the 3-effect MEDs equipped with the developed wick-free plate produce 4.4% more freshwater than those with existing wick-plate.

Keywords: Multi-effect diffusion still; Solar energy; Distillation; Solar still; Effect plate

1. Introduction

Solar still is a device that produces freshwater by evaporating seawater or brackish water using solar thermal energy. Solar stills are divided into a passive type that directly uses solar thermal energy and active type that indirectly uses solar thermal energy through the solar collector, pump, and heat exchanger. The former has a simple structure and high maintainability, but its production amount is low. Although the latter has higher productivity, there are disadvantages that the additional devices are introduced, causing the lower maintainability and the higher installation cost. In this study, we focused on the passive solar still which can be used by people without expert knowledge and living in remote areas where infrastructure for electricity and water is not built or limited. Multi-effect diffusion solar still (MED) employed in this study can be expected to produce freshwater of about 20 kg/(m² d) despite the passive type solar still with a simple structure.

* Corresponding author.

In 1959, Telkes [1] developed the MED to increase low productivity of 2–5 kg/(m² d) of conventional solar still. The MED obtained distillate by the temperature difference between plates installed in parallel (Fig. 1). Each effect consists of a plate and a wick. The wick is mostly made of cotton or jute cloth and attached to the rear surface of each flat plate. The feed water flows down slowly through the wick from the top side of the MED and spreads over the entire surface of the wick to secure sufficient evaporation time and area. When solar energy is absorbed in the first black plate through the cover glass, the solar thermal energy is transferred to seawater flowing down through the wick and evaporates the seawater. Evaporated water vapors diffuse across a small gap between the effects and condense on the next plate surface. The latent heat generated by the condensation is utilized as the heat source of the next plate and transfers to the last plate through the evaporation-diffusion-condensation process. This phenomenon repeats at each effect and leads to an increase in production. In addition to Telkes [1], Cooper and Appleyard [2] and Ouahes et al. [3] fabricated the MED and obtained distillate of 15 kg/(m² d) through experiments. Many researchers have been developing various types of the MED that applied additional reflectors [4,5] to the inside and outside of the device, combined the basin still and the MED [6], and combined tilted wick still [7]. Many studies have also been conducted to optimize the diffusion gap, the installation angle, and the feed flow rate for improvement of the productivity of the MED [8–12]. Most of the MED use wicks as an evaporating surface.

However, the use of the wicks to the effect plate can cause some problems. The detachment of the wick due to the decrease of the adhesive strength of the adhesive sheet and thermal deformation of the plate over time causes the mixing of feed seawater into the condensate of the next plate surface, which decreases performance and the quality of the production water. The low thermal conductivity of the wick itself increases the thermal resistance of each effect. The use of wicks also increases the fabrication process time and cost to attach onto the plate. Therefore, it is necessary to develop a MED with a simplified structure without the wick.
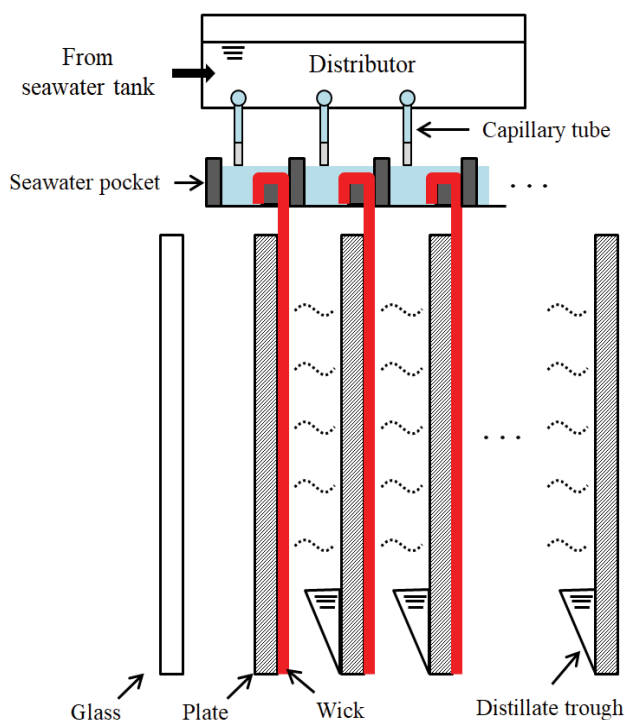
In this study, we have developed a so-called wick-free plate, which has similar performances to the wick-plate. Successful development of the wick-free plate can improve the maintainability and reliability of the MED by securing the structural simplicity, the efficiency of production, and the performance improvement.

2. Required characteristics of wick-free plate

The required characteristics for a wick-free plate are summarized from those of wick-plate as following seven characteristics: falling water velocity (V_f), spreadability (S_f), thermal conductivity, seawater corrosion resistance, heat resistance, fabrication cost, and processability. Table 1 shows the specifications of the wick-plate as a reference for each characteristic value. The total thickness of the wick-plate, including the adhesive to bond the wick to the plate, is 1.5 mm and the thermal conductivity of wick is the lowest among the wick-plate components. When the seawater flows down along the evaporation surface, the flow characteristics such as falling water velocity V_f and spreadability (wetting area) are strongly related to the performance of the MED. The V_f is defined as the velocity at which the seawater supplied from the top of the plate flows down to the bottom. The S_f refers to how much seawater spreads in the width direction on the plate and can be defined as a wetted area by the seawater relative to the available evaporation surface area of the plate. In this study, we calculated the ratio of the wetted area to the plate evaporation area through an image process after taking pictures at a steady state. The S_f has a mutual influence on the V_f and is directly proportional to the evaporation area, so this factor affects the evaporation amount, which is related to the freshwater production.

The productivity of the MED increases with an increase in temperature difference between the effects. The conductive heat transfer equation is presented in Eq. (1). The lower thermal resistance R can increase the temperature difference ΔT between effects at constant heat flux $\dot{Q}$. In addition, the lower thickness L and the higher thermal conductivity k of the plate can decrease the R and then increase the productivity.

$$\dot{Q} = \frac{\Delta T}{R} \tag{1}$$

where $R = \dfrac{L}{kA}$.

The wick-free plate is considered to be an integrated plate without both wick and adhesive. Therefore, it is necessary to consider not only the k but also the L of the

Fig. 1. Schematic diagram of MED.

Table 1
Specifications of wick-plate

Component	Wick	Adhesive	Plate
Thickness (mm)	0.8	0.2	0.5
Thermal conductivity (W/m K)	0.25	0.33	16.5
Material	Cotton	Polypropylene	STS 316L
Cost ($/m²)		15	
Processability		Bad (Purchase & Attachment process)	
Seawater resistance		Good (Characteristics of STS 316L)	
Heat resistance		Good (Characteristics of STS 316L)	

wick-free plate. In addition, it should be considered that diffusion resistance in the diffusion gap between plates is a dominant factor affecting freshwater yield.

The corrosion resistance of materials to seawater is the most basic requirement for equipment using seawater. The seawater corrosion shortens the lifetime of the distiller and contaminates the distillates. Corrosion resistance characteristics of the wick-free plate materials should be equivalent level to the wick plate, STS316L. The STS316L is generally acceptable materials for seawater corrosion resistance considering its cost. Most of these metal materials show a sufficient heat resistance and apply to the MED operating typically under 100°C.

Since this study was carried out considering the commercialization of the MED, it is important to evaluate not only the performance of the device but the fabrication cost. In the same vein, the processability is also an important factor to be considered. The processability refers to the easiness level of processing for the plate to be the desired form. When the processability is poor, it is hard to be formed to desired shapes of the plate and causes increases in manufacturing cost.

In this study, we have focused on two important factors (V_f and S_f) of 7 factors above mentioned, because the others can be evaluated by qualitative analysis relative to the wick-plate and investigation from the market.

3. Fabrication of wick-free plate

The manufacturing cost is greatly affected by the material and processing method. Therefore, it is necessary to first select materials and structures that have similar performance to wick-plate by considering such factors as thermal conductivity, seawater corrosion resistance, heat resistance, and processability. Materials such as stainless steel, thermally conductive plastic, and aluminum may be satisfied with the required characteristics. Among them, thermally conductive plastic and aluminum are advantageous because they can be applied to injection and extrusion processes and causes lower unit cost by mass production. However, in this paper, stainless steel was preferred as the candidate material because of the expensive mold cost for the injection and extrusion processes.

The V_f and S_f among the wick-free plate requirements directly affect the evaporation time and evaporation area of seawater. Since the wick is a porous structure, feed water spreads slowly and uniformly on that structure by capillary force, so sufficient evaporation time and area can be secured. We proposed three types, that is, mesh type, sintered surface type, and grooved surface type (2-dimensional embossing structure) to materialize these advantages of the wick.

A condensation surface of the effect plate should be seamlessly and smoothly flat to effectively collect condensed droplets. Therefore, the one side surface of a mesh-type specimen should be flat by using a metal plate or thin film. However such a structure is substantially not different from the wick-plate structure attaching a fabric wick to the metal plate. In addition, making an all-in-one plate that has a smooth surface on one side and mesh surface on the other side is practically difficult unless customized. However, since the commercially available Ni or Ti porous metal mesh is very cheap, light, and has excellent thermal conductivity, it is possible to form an effective effect plate by forming a condensation surface on one side. In the case of porous mesh type, three specimens with different density and material were prepared as shown in Table 2. The dimension of all specimens is 200 mm × 400 mm except PO3T which is 300 mm × 300 mm.

In the case of the sintered surface type, it is difficult to make only the evaporation surface porous while keeping the condensation surface smooth, and expensive to make only a few specimens. Therefore, in this study, the grooved surface type was mainly considered in the shape of the wick-free plate (Fig. 2) and focused on optimizing the patterned groove shape to have comparable performance with the wick-plate.

Various shapes such as wave, vertical, rectangular, triangular, and oblique groove can be considered, but the binary rectangular type (Fig. 2a) is the most appropriate surface shape considering V_f, S_f, and processability. Fig. 3 shows the wick-plate specimen (Fig. 3a) as reference for comparison, the groove type specimens by etching and 3D printing (Figs. 3b and c), and porous metal specimens (Fig. 3d). The groove by etching is semi-cylindrical shape due to the method by chemically eliminating surface. The ridge of the groove by 3D printing can be inclined with an arbitrary angle (60°) as shown in Fig. 3c.

There are various methods to make groove shape using stainless steel such as welding, etching, 3D printing, and fin forming. Since the MED can yield more distillate at the narrower diffusion gap, dimensions of the patterned groove are very small as a few millimeters. Therefore, welding many rectangular bars on a flat surface is inefficient to make patterned grooves. In the case of fin forming, it was possible to make various shapes but difficult to get a small number of specimens because fin forming is suitable for mass

Table 2
Specimen name and specifications of wick-free plate

	Type	Specimen name	Specification (mm)	Thickness (mm)	Thermal conductivity (W/m K)	Remark
Wick-plate		W4	N/A	1.5	0.25	N/A
Groove	3D printing	3D421	4.0P 2.0F 1.4D	3.4	16.5	STS316L
		3D422	4.0P 2.0F 2.0D	4		
		3D631	6.0P 3.0F 1.4D	3.4		
		3D632	6.0P 3.0F 2.0D	4		
	Etching	E421S	4.0P 2.2F 1.4D	2	16.5	
		E631S	6.0P 3.1F 1.4D			
		E632S	6.0P 3.3F 2.0D			
		E422	4.0P 2.0F 2.0D			
		E432	4.0P 3.0F 2.0D			
		E422S	4.0P 2.0F 2.0D			
		E432S	4.0P 3.0F 2.0D			
		E442	4.0P 3.6F 2.0D			
		E332	3.5P 2.7F 2.0D			
Porous metal		PO1N	N/A	1.1	90.9	280 g/m^2 (Ni)
		PO2N	N/A	2.1		450 g/m^2 (Ni)
		PO3T	N/A	1.5	21.9	5 μm (Ti)

'S' at the specimen's name denotes the etched specimen on the whole evaporation area by the second etching process.
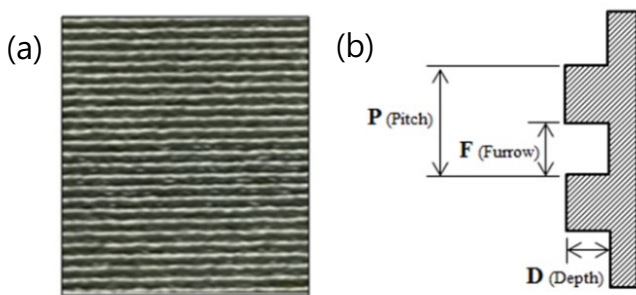
Fig. 2. Groove shapes of evaporating surface for wick-free plate.

production. Therefore, 3D metal printing and etching methods were used to fabricate specimens with various groove sizes (depth, width, and pitch).

Table 2 shows the identifications of the prepared groove and porous metal specimens, shape specifications, and thermal conductivity. In the specimen specification, the P, F, and D mean pitch (distance between grooves), furrow (width of the groove), and depth (depth of the groove), respectively as shown in Fig. 2b. The groove dimension (F = 2.0–3.6 mm, D = 1.4–2.0 mm) was selected by considering the lateral S_f of seawater in the groove. If the furrow is less than 1 mm, the water in the groove is dominated by the capillary force rather than momentum by gravity [13]. Therefore, due to the surface tension, the supplied water droplets may not smoothly spread in the lateral direction in the grooves. On the contrary, if the F is too large, gravity is the dominant force causing excessive falling velocity of water droplet resulting in short evaporation time. Further, the seawater in the grooves receives not only the capillary force and gravity

but also the momentum from the supplied seawater, which also affects the lateral S_f. Therefore, the dimensions of the groove are limited by the capillary force and flow rate of supplied seawater and the groove is physically designed to act as a weir. Meanwhile, an 'S' at the specimen ID denotes the etched specimen on the whole evaporation area by the second etching process to confirm an effect with the roughness of the surface.

4. Experimental results and discussions

4.1. Falling water velocity and spreadability

Experiments were carried out to determine V_f and S_f among the required characteristics of the wick-free plate presented in Section 2.

The specimens used in these experiments are shown in Table 2. As shown in Fig. 4, the specimen was mounted vertically, and then dyed tap water was supplied with a syringe pump at a constant flow rate on the center of the upper part of the specimen. The water flow rate was 1.6 ml/min for all experiments based on a previous study [14]. The V_f was calculated by measuring the duration at which the first droplet fell from the bottom of the wick or specimen after the seawater was supplied. Experiments were carried out in a constant ambient temperature of 23°C ± 2°C and humidity of 55% ± 5%.

Table 3 and Fig. 5 shows the experimental results on the V_f and S_f. As shown in Fig. 5a, the V_f s of some of the specimens except for porous metal specimens were lower than that of the wick-plate specimen. The S_f s of all specimens were lower than that of the wick-plate specimen as shown in Fig. 5b.
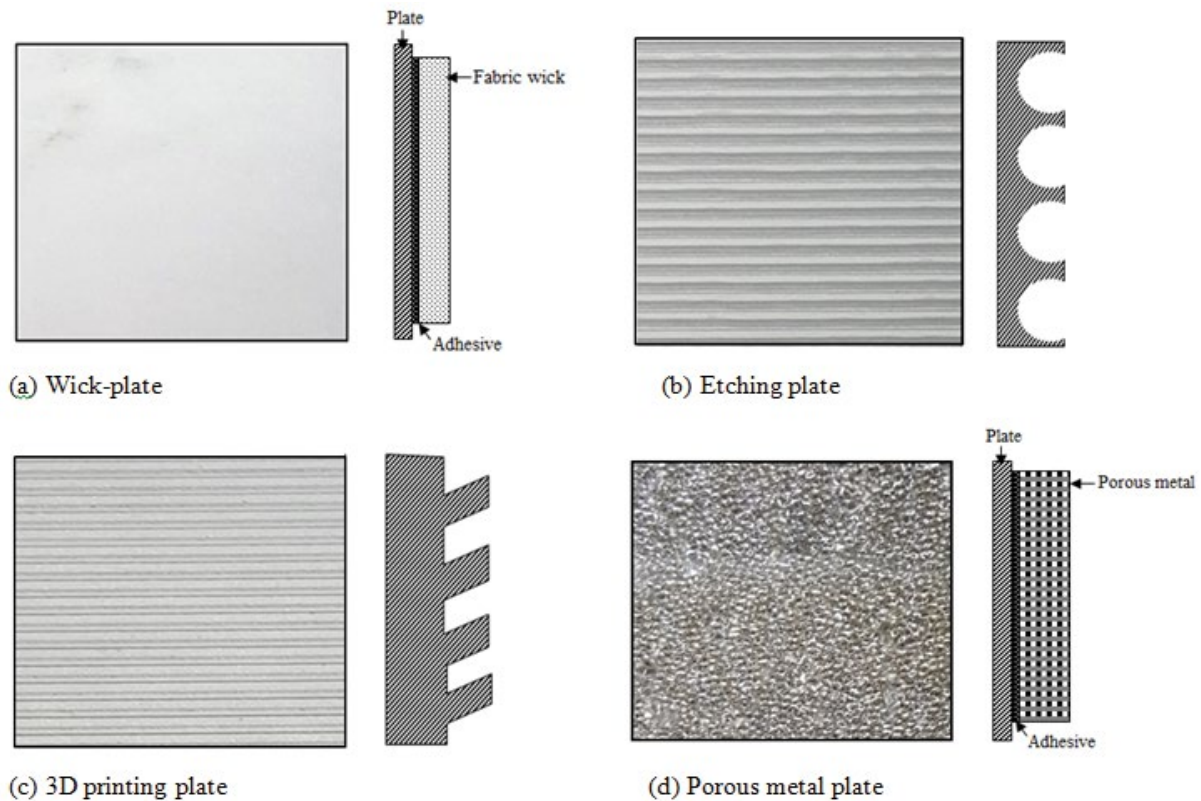
Fig. 3. Wick-plate and various wick-free plates of MED.
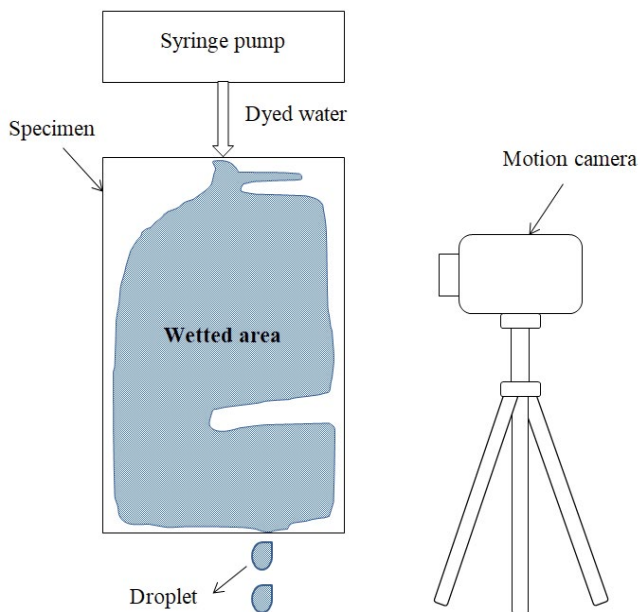
Fig. 4. Experimental setup for measuring falling water velocity and wetted area.

For the 3D printing specimens, the V_fs was 0.26–0.36 mm/s and slower than the wick-plate specimen (0.44 mm/s). Considering the groove area ratio of a maximum of 50%, the wetted or effective evaporation area was half of the total plate area. Actually, when seawater flows down on the specimen, the seawater is firstly filled in the first furrow, passes on the ridge part as a streak form of water, and then is fed to the next furrow. Therefore, this wetted area ratio of 50% is the minimum value that can be read by the photograph because a part surface on the ridge is also locally wet. The results showed that the surface roughness was related to the S_f. As shown in Fig. 6, the surface of the 3D printing specimen (Fig. 6a) is rougher than that of etching plate specimen (Fig. 6b). When comparing results of 3D422 to E422 with the same dimension, the S_f of 3D422 is better than that of E422 as shown in Table 3. This means the rough surface helps the water to spread well.

In the case of porous metals, except for PO1N, the V_fs were 8.5–11.6 mm/s, which was 19.3–26.4 times faster than wick-plate and the S_f was below 37%. The wetted area of PO2N is invisible with a photograph or naked eyes because the seawater was penetrated the inner porous structure, but it was estimated to be fewer than 37% in terms of V_f and S_f. Although the performance of the spreadability of the porous metal specimen is lower than that of other wick-free plate candidate specimens, the weakness may be compensated by an increase of overall heat transfer due to area porous structure and higher thermal conductivity of 66–364 times of wick-plate.

In the case of the etching type specimens, the falling water velocities varied from 0.17 to 8.6 mm/s and the S_f varied from 3% to 71% depending on the shape dimensions of the grooves (Table 3). Fig. 7 shows V_f and S_f for etching type specimens. The S_f is higher for the specimens with lower V_f.

Table 3
Falling water velocity and wetted area ratio of specimens

Type	Specimen ID	Specification, mm	Falling velocity, mm/s	Wetted area ratio, %
Wick	W4	–	0.44	100
3D printing	3D421	4.0P 2.0F 1.4D	0.36	44
	3D422	4.0P 2.0F 2.0D	0.29	50
	3D631	6.0P 3.0F 1.4D	0.26	42
	3D632	6.0P 3.0F 2.0D	0.34	34
Etching	E421S	4.0P 2.2F 1.4D	6.20	–
	E631S	6.0P 3.1F 1.4D	8.60	–
	E632S	6.0P 3.3F 2.0D	3.89	3
	E422	4.0P 2.0F 2.0D	0.50	24
	E432	4.0P 3.0F 2.0D	0.19	58
	E422S	4.0P 2.0F 2.0D	3.52	3
	E432S	4.0P 3.0F 2.0D	0.63	10
	E442	4.0P 3.6F 2.0D	1.06	6
	E332	3.5P 2.7F 2.0D	0.17	71
Porous	PO1N	–	36.0	1
	PO2N	–	11.6	Unrecognizable
	PO3T	–	8.50	37
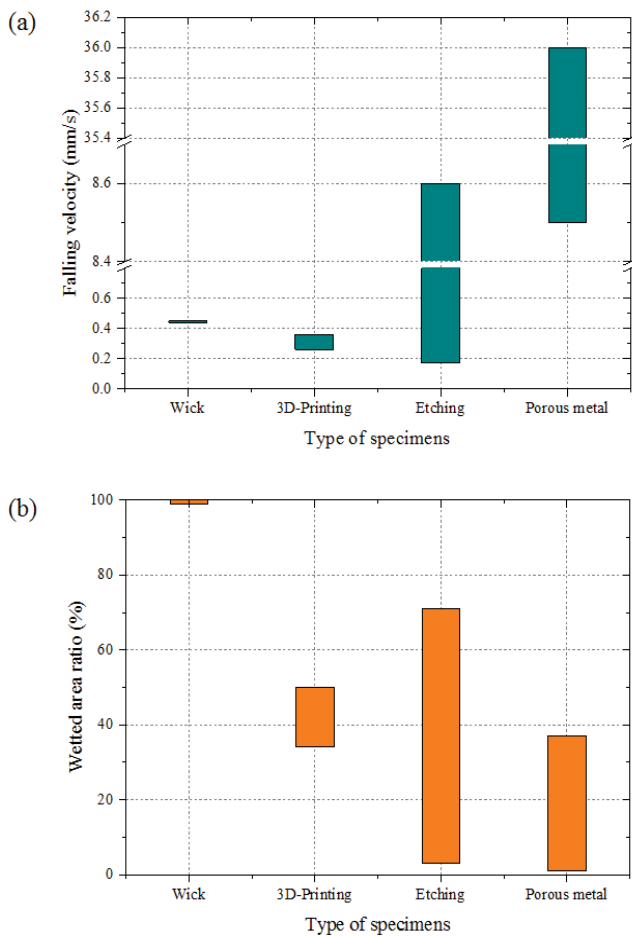
Fig. 5. Characteristics with type of specimens (a) falling water velocity and (b) wetted area ratio.

This result showed these two factors are closely related to each other and are almost inversely proportional. Therefore, both of V_f and S_f might be evaluated by comparing either of the two characteristics. In addition, the specimens including 'S' in the specimen ID which etched on whole surface area by secondary etching process showed poor V_f and S_f characteristics. This result may be caused by the effect of the edge shape of the groove rather than the surface roughness. As shown in Fig. 6b and Fig. 3b, the E422 has a sharp edge in the ridge so that the supplied water can be filled and stagnate in the groove. However, as shown in Fig. 6c, the additional processing made the edges less sharply, causing the water to flow down into the next groove before spreading.

Fig. 8 shows V_f in the groove shape of the etching type specimens. By comparing the results of E432S, E422S, E432, and E422 in Fig. 8a, V_f decreases as F increases. As can be seen in Fig. 8b, the E421S and E422S, and E631S and E632S results show that the V_f decreases with the increase of D. Comparing the results for E632S, E432S, and E332 from Fig. 8c, it can be seen that the smaller value of P shows the lower the V_f under the same conditions of F and D. Therefore, the smaller P, the larger F, and the greater D get the better V_f characteristics. However, the results for E442 ($F = 3.6$ mm), E432 ($F = 3.0$ mm) and E422 ($F = 2.0$ mm) show that the V_f increases when F is increased at larger value than 3.0 mm at constant $P = 4$ mm. This may be attributed to the fact that the capillary force to seize the water in both groove side walls is smaller at a larger size than 3.0 mm. Considering E332, it can be estimated that F of 2.7–3.0 mm belongs to the optimal range. Therefore the optimal patterned groove dimension is selected as $P = 3.5$ mm, $F = 2.7$ mm, and $D = 2$ mm through the experimental results and the above analysis.

The etching plate (E332) has 71% of S_f of the wick-plate and lower falling velocity (0.17 mm/s) than the wick-plate.

(a) 3D printing plate　　(b) Normal etching plate (E422)　　(c) Additional etched plate on the entire etching plate surface (E422S)
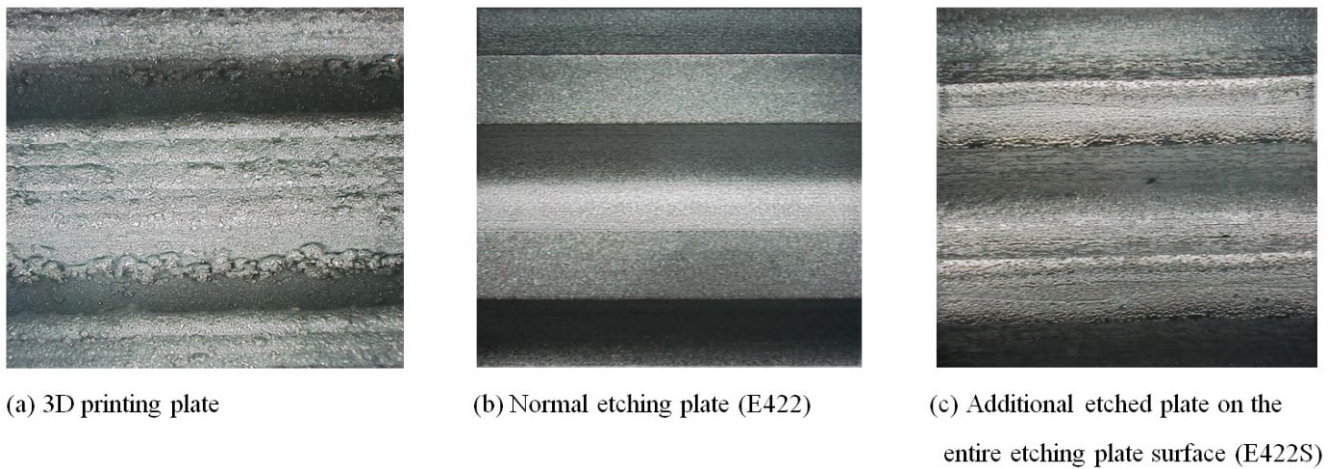
Fig. 6. Scanning electron microscopy images of 3D printing and etching specimens.
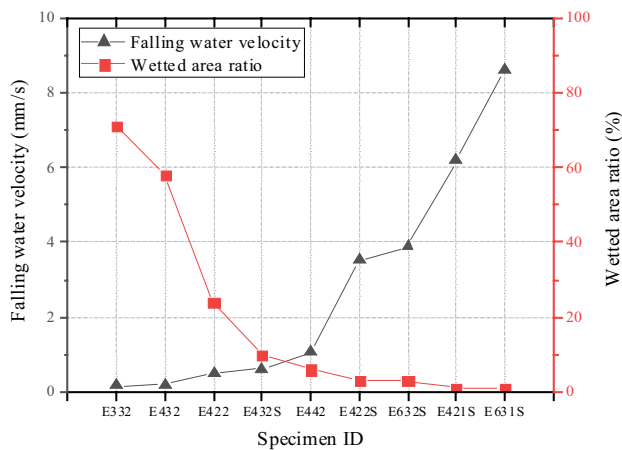
Fig. 7. Falling water velocity and wetted area ratio of each etching specimen.

This is regarded as the best characteristics among all wick-free plate specimens. Furthermore, this has better processability than porous metal plate specimens that need attaching process in fabrication and has a much lower cost than 3D printing specimens. Thus, the etching plate specimen (E332) was selected as the wick-free plate in this study.

4.2. Productivity comparison of MEDs

Preliminary experiments for productivity between MEDs using the selected wick-free plate and wick-plate respectively were conducted to confirm their performance. The MEDs consisted of 3-effects using each plate and were fabricated in a similar setup to Fig. 1. The experiment was carried out at the Korea Institute of Machinery and Materials, Daejeon, Republic of Korea for 2 d from November 3 to 4, 2018, at 10 and 10.5 MJ/d of solar radiation and 17.4°C and 18.2°C of average ambient temperature. The MED applied with a wick-free plate produced 3.22 and 3.55 kg/d of freshwater, respectively, and the MED with wick-plate produced 3.09 and 3.4 kg/d, respectively. These results indicate that the MED with a wick-free plate is produced 2.5–4.4% more than MED with the wick-plate.

5. Summary and conclusions

This study described the process and experimental results of the development of a wick-free plate not to apply the wick, which is a key component of MED. The required characteristics of wick-free plate specimens were arranged based on the characteristics of the wick-plate. The falling water velocity (V_f) and spreadability (S_f) in the evaporating surface, which are the main characteristics, were obtained through experiments. The productivities of the MEDs with wick-free plate and wick-plate were also compared from the outdoor experiment. We finally developed a wick-free plate through this experiment and the conclusions obtained from the experimental results are as follows.

The final selected specimen as the wick-free plate is an etching plate (E332), which is the groove type specimen with the best characteristics of V_f and S_f. It was confirmed that V_f and S_f of groove type were excellent when there are smaller pitch and deeper depth. Furthermore, the experimental results show that the furrow has an optimal range. The optimum shape of the groove is 3.5 mm for the pitch, 3.0 mm for the furrow, and 2.0 mm for the depth. In the results of the outdoor performance experiment for 3-effect MEDs with the developed wick-free plate and existing wick-plate, the MED with wick-free plate produces 2.5–4.4% more freshwater than those with existing wick-plate. Therefore, the wick-free plate has been successfully developed, which can make the MED not only more reliable and maintainable by securing structural simplicity but also more productive.

Acknowledgments
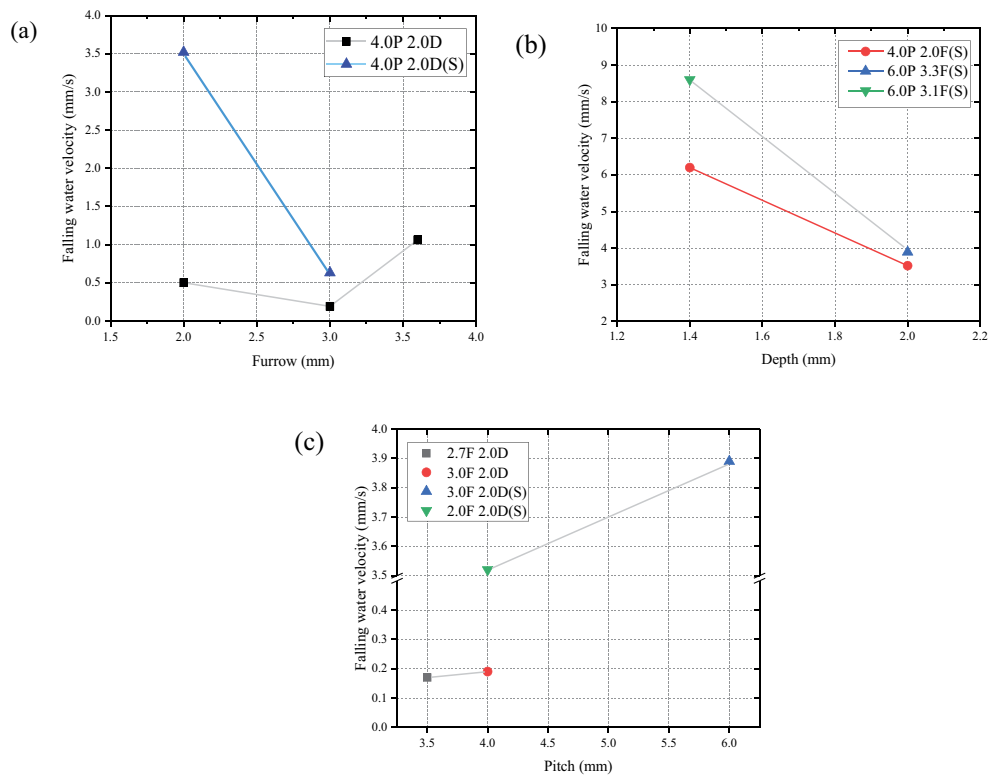
Fig. 8. Falling water velocity with groove shape (a) furrow, (b) depth, and (c) pitch.

References

[1] M. Telkes, Solar Still Construction, OSW Research and Development Progress Report, 33 (1959).

[2] P.I. Cooper, J.A. Appleyard, The construction and performance of a three-effect, wick-type, tilted solar still, Sun at Work, 12 (1967) 4–8.

[3] R. Ouahes, C. Ouahes, P. Le Goff, J. Le Goff, A hardy, high-yield solar distiller of brackish water, Desalination, 67 (1987) 43–52.

[4] H. Tanaka, Experimental study of vertical multiple-effect diffusion solar still coupled with a flat plate reflector, Desalination, 249 (2009) 34–40.

[5] C.D. Park, B.J. Lim, Y.D. Noh, S.S. Lee, K.Y. Chung, Parametric performance test of distiller utilizing solar and waste heat, Desal. Wat. Treat., 55 (2015) 3303–3309.

[6] H. Tanaka, T. Nosoko, T. Nagata, Experimental study of basin-type, multiple-effect, diffusion coupled solar still, Desalination, 150 (2002) 131–144.

[7] H. Tanaka, K. Iishi, Experimental study of a vertical single-effect diffusion solar still coupled with a tilted wick still, Desalination, 402 (2017) 19–24.

[8] H. Tanaka, T. Nosoko, T. Nagata, Parametric investigation of a basin-type-multiple-effect coupled solar still, Desalination, 130 (2000), 295–304.

[9] H. Tanaka, T. Nosoko, T. Nagata, A highly productive basin-type-multiple-effect coupled solar still, Desalination, 130 (2000) 279–293.

[10] B.J. Lim, S.S. Yu, C.D. Park, K.Y. Chung, One-dimensional numerical analysis of the effect of seawater feed rate on multi-effect solar stills, Korean Soc. Mech. Eng. B, 40 (2016) 477–484.

[11] B.J. Lim, S.S. Yu, K.Y. Chung, C.D. Park, Numerical analysis of the performance of a tiltable multi-effect solar distiller, Desalination, 435 (2018) 23–34.

[12] H. Tanaka, Theoretical analysis of a vertical multiple-effect diffusion solar still coupled with a tilted wick still, Desalination, 377 (2016) 65–72.

[13] J.C. Berg, An Introduction to Interfaces & Colloids: The Bridge to Nanoscience, World Scientific publishing Co., Singapore, 2010.

[14] C.D. Park, B.J. Lim, K.Y. Chung, S.S. Lee, Y.M. Kim, Experimental evaluation of hybrid solar still using waste heat, Desalination, 379 (2016) 1–9.